P.J. Pinzón, I. Pérez, C. Vázquez, J. M. S. Pena (2014). "Broadband 1×2 Liquid Crystal Router with Low Thermal Dependence for Polymer Optical Fiber Networks. In *Optics Communications*, Volume: 333, Issue: 15, Pages: 281-287. Available in http://dx.doi.org/10.1016/j.optcom.2014.07.065

Broadband 1 × 2 liquid crystal router with low thermal dependence for polymer optical fiber networks

Plinio Jesús Pinzón*, Isabel Pérez, Carmen Vázquez, José Manuel Sánchez-Pena

Grupo de Displays y Aplicaciones Fotónicas, Dpto. de Tecnología Electrónica, Universidad Carlos III de Madrid, C/Butarque 15, 28911 Leganés, Madrid, Spain

Abstract: A 1 × 2 optical router based on an achromatic liquid crystal polarization rotator has been designed and experimentally tested. The router can work in the spectral range used in step-index polymer optical fiber networks (400–700 nm) with low wavelength and temperature dependences. The theoretical design is fast and simple and has good agreement with experimental results. Experimental crosstalk is lower than −18.68 dB for both outputs, even with thermal variations of 10 °C. Performance improvement with respect to previously reported devices with similar structure has also been analyzed.

Keywords: Optical router, Liquid-crystal device, Polarization-selective device, Fiber optics communications, Multiplexing, Variable optical splitter.

1. Introduction

Polymer optical fibers (POFs) have been reported as one of the most promising transmission media for short distance communication networks. Today, POF is displacing copper step by step, especially in the automotive industry, because it saves more space and weight and offers immunity to electromagnetic interferences. POFs are also a low cost solution for the development of short-range high-speed data networks, as in home and office networks, for the ease of making connections since they have higher dimensions, larger numerical aperture and larger critical curvature radius, in comparison with glass optical fibers, which allows the necessary curvatures in the wiring of home networks [1]. Moreover, it has been shown that POFs have multiple applications in sensor systems at low or competitive cost compared to the well-established conventional technologies [2].

To date, most used POF type is the step-index POF (SI-POF). It is made of polymethyl-methacrylate (PMMA) and it is also called standard POF. SI-POF has 980 μm core diameter, 10 μm cladding thickness and 0.5 numerical aperture (NA). SI-POF has high modal dispersion, which reduces the usable bandwidth to 14 MHz × 100 m. And it is only used in visible spectrum range (VIS), where it can provide acceptable attenuation (e.g. 100 dB/km at 650 nm) [3].

* Corresponding author. Tel.: +34 916249197; fax: +34 916249430.
E-mail addresses: ppinzon@ing.uc3m.es (P.J. Pinzón), isaper@ing.uc3m.es (I. Pérez), cvazquez@ing.uc3m.es (C. Vázquez), jmpena@ing.uc3m.es (J.M. Sánchez-Pena).

Initially, transmission with SI-POF has been realized with only one wavelength, reaching speeds of 100 Mb/s over links of 275 m [4], even multi-gigabit transmission over links of 50 m has been reached [5]. However, in the last years, wavelength division multiplexing (WDM) has been proposed as one potential solution to expand the usable bandwidth of POF based systems [6,7]. In the same way, many POF based sensors implement self-referencing schemes by transmitting different wavelengths over a single fiber [2]. These techniques require the development of devices capable of multiplexing, demultiplexing and routing optical signals in a broadband range, in order to cover the proposed SI-POF WDM spectral grid (400–700 nm) [8]. These optical devices are well established for WDM applications in the infrared range (IR) and near IR (NIR) [9]. However, they require a complete re-design for being implemented in SI-POF WDM systems.

Optical routers are key components in WDM networks. They selectively route optical signals delivered through one or more input ports to one or more output ports. Different technologies could be applied to route optical signals [10]. The final choice depends on the optical network topology, switching speed and spectral range required.

Liquid crystal optical routers (LC-ORs) are mainly based on polarization modulation in combination with polarization selective calcite crystals (PBS) to steer the light [10–12]. Main advantages of LC technology include no need of moving parts for routing reconfiguration, low driving voltage and low power consumption. The response time of nematic LC devices is usually in the order of several milliseconds, so they are ideal for protection and recovery applications and optical add/drop multiplexing, which demand

fewer restrictions on routing time. However, in the last years, nematic liquid crystal cells with response times lower than 3 ms [13] and 2 ms [14], as well as nanosecond response [15] and different techniques to reduce the response time below 1 ms [16] have been reported. On the other hand, ferro-electric (FE) LC offers response times in the order of micro-seconds but their operation is limited to the on/off states (bistable) [17,18].

Usually, and especially in applications where channel equalization is needed, LC-ORs use twisted nematic (TN) LC cells, acting as polarization rotators (PRs) with a continuous operation mode (intermediate transmission levels) [19,20]. However, their performance is optimum only for specific wavelengths (Mauguin Minima) [21]. Besides, the LC birefringence, which defines Mauguin Minima, is very temperature dependent [22], requiring temperature compensated designs or controllers. These are important limitations even in the most recent published LC devices [23].

In this work, a broadband 1 × 2 LC-OR with low thermal dependence based on an achromatic PR is presented. The PR design is done by using a simple computational optimization approach with a good performance versus more complex approaches [24,25]. The PR design is based on three nematic LC cells, and it is done in order to have optimum response across the 400–700 nm spectrum. The router performance, measured in terms of insertion loss and crosstalk, is experimentally tested in the range from 400–700 nm and it is compared against the performance of a router based on a single TN cell, named simple router. It is also demonstrated, by simulation results, that the proposed router allows splitting the input signal between the output ports with adjustable split ratio and low wavelength dependence, and that it offers a very low dependence with the temperature in a broadband range thanks to its spectral uniformity.

2. Polarization rotators

PRs modify the orientation of a linear polarized beam in a specific angle, e.g. from being *x*-polarized to be *y*-polarized. The most common PR scheme consists of a single TN cell, while achromatic or broadband designs include TN cells, retardation plates and/or homogenous nematic (HN) LC cells [24–28].

2.1. Nematic liquid crystal cells operation and modeling

The operation of a nematic LC cell is based on the optical birefringence, Δn, between the fast and slow axes of its molecules (slow axis is called *c*-axis); see Fig. 1a. A HN cell, with thickness d_H and birefringence Δn_H, produces a phase delay between the polarization components of a light beam, with wavelength λ, that is given by

$$\Gamma_H = 2\pi \frac{\Delta n_H d_H}{\lambda} \tag{1}$$

hereinafter, the sub index *H* can be replaced by *T*, in order to refer to a TN cell.

The birefringence wavelength dependence, $\Delta n(\lambda)$, is a very important parameter for designing broadband devices with stacked structures [25,29]. In this work, $\Delta n(\lambda)$ is represented with the extended Cauchy model [22], which is expressed as

$$\Delta n(\lambda) = A_{eo} + \frac{B_{eo}}{\lambda^2} + \frac{C_{eo}}{\lambda^4} \tag{2}$$

where A_{eo}, B_{eo} and C_{eo} are the differences between the extraordinary and ordinary Cauchy coefficients $A_e - A_o$, $B_e - B_o$ and $C_e - C_o$, respectively.

The LC *c*-axis angle with respect to the cell surface is defined as the tilt angle, θ. Without applied voltage, HNs and TNs cells have $\theta \cong 0^\circ$ (usually a pre-tilt angle is added). In a HN cell (see Fig. 1b) the front and rear molecules have the same orientation angle, while in a TN cell (see Fig. 1c) there is a twist angle, ϕ_T, between them. Therefore, HN cells are a particular case of TN cells without twist angle, and their Jones matrix representation [21] is given by

$$W_H(\alpha_H) = R^{-1}(\alpha_H) \times \begin{bmatrix} e^{-i(\Gamma_H/2)} & 0 \\ 0 & e^{i(\Gamma_H/2)} \end{bmatrix} \times R(\alpha_H) \qquad 3)($$

where $R(\alpha_H)$ is the rotation matrix of the LC *c*-axis azimuth angle, α_H, with respect to the *x*-axis (see Fig. 1b), and it is given by

$$R(\alpha_H) = \begin{bmatrix} \cos(\alpha_H) & \sin(\alpha_H) - \\ \sin(\alpha_H) & \cos(\alpha_H) \end{bmatrix} \tag{4}$$

And the Jones matrix of a TN cell [21], with its front *c*-axis oriented at an azimuth angle α_T and with a total twist ϕ_T, is given by

$$W_T(\alpha_T) = R^{-1}(\alpha_T) \begin{bmatrix} \cos(\phi_T) & - \sin \\ (\phi_T) \sin(\phi_T) & \cos(\phi_T \end{bmatrix} \begin{bmatrix} \cos(X) - i\frac{\Gamma_T}{2}\frac{\sin(X)}{X} & \phi_T \frac{\sin(X)}{X} \\ -\phi_T \frac{\sin(X)}{X} & \cos(X) + i\frac{\Gamma_T}{2}\frac{\sin(X)}{X} \end{bmatrix} R(\alpha_T) \qquad 5)($$

where $X = [\phi_T^2 + (\Gamma_T/2)^2]^{1/2}$. The elements {1,1} and {2,1} of Eqs.(3) and (5) represent the output *x*-polarized and *y*-polarized components (T_x and T_y), respectively, when the input beam is *x*-polarized.

2.2. Single twisted nematic cell based polarization rotator

A TN based PR consists of a TN cell bounded between linear polarizers, LPs, parallels to the LC front and rear *c*-axes. Most common design uses a TN cell with 90° twist, e.g., assuming $\alpha_T = 0^\circ$, input and output LPs are parallel to the *x*-axis and *y*-axis, respectively (crossed LPs). In this configuration with no applied voltage (*V*), from Eq. (5), an input *x*-polarized beam is transmitted

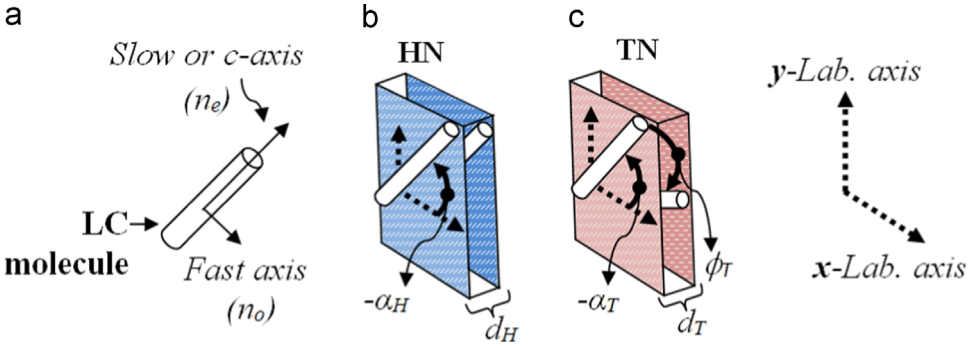

Fig. 1. Nematic LC cells representation: a) nematic LC molecule, b) homogeneous nematic LC cell (HN) and c) twisted nematic LC cell (TN).

with y-polarization direction, as shown in Fig. 2a, according to

$$T_y = \cos(B)^2 + \left(\frac{\Gamma_T}{2}\frac{\sin(B)}{B}\right)^2 \quad (6)$$

with $B=[(\pi/2)^2+(\Gamma_T/2)^2]^{1/2}$. T_y from Eq. (6) presents periodic peaks at the Mauguin minima, given by

$$\frac{\Delta n_T d_T}{\lambda} = \frac{1}{2}\sqrt{4N^2-1} \text{ with } N = 1, 2, \ldots \quad (7)$$

When V is higher than a threshold value, V_{th}, the LC molecules are tilted in the resulting electrical field direction ($\vec{E}$), $0^\circ < \theta < 90^\circ$, and they are parallel to $\vec{E}$ when $V \gg V_{th}$, then $\theta \sim 90^\circ$, $\Delta n_T = 0$ and $\Gamma_T \sim 0$; hence, there is not a polarization rotation and light is blocked, as shown in Fig. 2b. Fig. 3 shows the transmittance or rotation efficiency, T_y, in the range from 400–700 nm of two PRs, based on 5 μm and 15 μm thickness TN cells filled with commercial 5CB material. The 5 μm TN cell based PR has $T_y \geq 88\%$. The efficiency is improved to $T_y \geq 98\%$ using a 15 μm TN cell, which can be considered as an achromatic design, but the response time, τ, in this case is 9 times the τ of the 5 μm cell, since $\tau \propto d^2$ [26]. Typically, a 5 μm TN cell has $\tau \sim 20$–30 ms [24]. Therefore, others achromatic PR designs are needed in order to improve the LC-ORs' spectral response, without increasing the response time.

2.3. Achromatic polarization rotators

Many approaches have been proposed for designing achromatic PRs, with structures equivalent to that shown in Fig. 4. Some designs are based on multiple TN cells, as the one reported in [26] with experimental $T_y \geq 92\%$ in the VIS using two TN cells of 20 μm thickness. Other designs are based on a TN between HN cells [25,28] or fixed retardation plates [24,27]. There have also been reported PRs based on ferro-electric LCs with a bistable operation and an almost achromatic response [18].

To our knowledge, the achromatic designs, based on Fig. 4 scheme, exposed in [24,25] present the best performance reported to date. They are based on optimization algorithms and have been done in the range from 400–700 nm. In [24], it is reported a design composed of a front retarder plate with $d_1 = 45.29$ μm and $\alpha_1 = 89.96^\circ$, a TN cell with $d_T = 6.20$ μm, $\phi_T = 90.12^\circ$ and $\alpha_T = 0^\circ$ of E7 LC mixture, and a rear retarder plate with $d_2 = 4.83$ μm and $\alpha_2 = -89.91^\circ$. The input LP is oriented at an azimuth angle $\beta = 1.64^\circ$. This PR presents $T_y \geq 97.8\%$ and it is designed after optimizing 7 variables (β, ϕ_T, α_1, α_2, d_T, d_1 and d_2). On the other hand, two designs using E7 LC material are reported in [25]. The first design is based on three TN cells between crossed LPs. The corresponding optimization includes thickness, azimuth and twist angles of each LC cell (9 variables). The optimal values are: $d_1 = 1.36$ μm, $\alpha_1 = -31.4^\circ$, $\phi_1 = 57^\circ$, $d_2 = 2.26$ μm, $\alpha_2 = -58.3^\circ$, $\phi_2 = 31.1^\circ$, and $d_3 = 1.54$ μm, $\alpha_3 = 59.9^\circ$, $\phi_3 = 62.9^\circ$, for cells 1, 2 and 3, respectively. The device has $T_y \geq 99.95\%$, which represents the best rotation efficiency reported to date. In the second design of [25], the cells 1 and 3 are HN (ϕ_1 and $\phi_3 = 0^\circ$) and the cell 2, which is placed between cells 1 and 3, is a TN cell. Then, 7 variables are used in this optimization and the optimal values are: $d_1 = 2.49$ μm, $\alpha_1 = -79^\circ$, $d_2 = 3.94$ μm, $\alpha_2 = 10.9^\circ$, $\phi_2 = 66.5^\circ$, $d_3 = 2.47$ μm, $\alpha_3 = -11^\circ$. This second device has $T_y \geq 98.87\%$. These designs are obtained with optimization algorithms that use between 7 and 9 variables. Optimization processes with fewer variables are often more effective and faster. They also consider LC cells with very specific parameters, complicating the manufacture of the PR and increasing its tolerances. These publications do not include experimental results. In the next section, the implementation of a broadband LC-OR based in an achromatic PR is described.

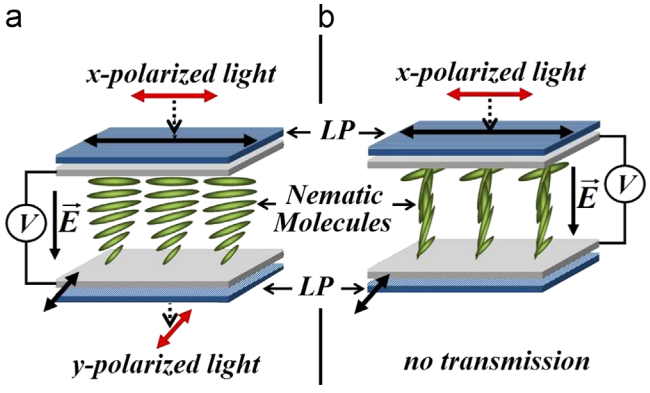

Fig. 2. TN cell based polarization rotator: a) $V < V_{th}$, b) $V \gg V_{th}$.

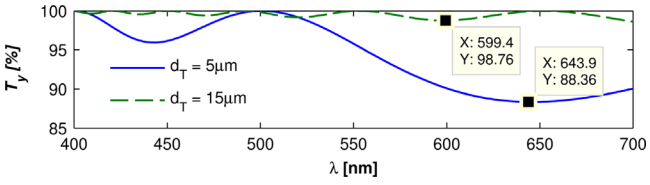

Fig. 3. Transmittance of a PR based on a TN cell of 5CB material with $d_T = 5$ μm and 15 μm.

3. Broadband 1 × 2 liquid crystal router

The proposed LC-OR scheme is shown in Fig. 5. It is composed by an input LP, parallel to the x-axis, an achromatic PR as polarization modulator, and an output polarization beam splitter (PBS).

3.1. Design of the achromatic PR

From the state-of-the art presented in Section 2.3 it can be seen that there are multiple configurations for designing achromatic PRs, which include TN cells, fixed retarder plates and variable retarder plates of HN cells and even of ferroelectric LC cells. However, the configuration based in a TN cell between HN cells offers one of the best polarization rotation efficiencies (T_y) and is less complex that the one based on 3 TN cells [25], so it is used in our design. Moreover, the design method is aimed to be simple and fast. So LC cells of the same material with fixed thickness are considered. It is also considered a TN cell with 90° twist in order to reduce the manufacturing complexity, since 90°−TN cells are very common and commercially available.

The achromatic PR is based on the scheme of Fig. 4. It is composed by three LC cells of 5CB material and 5.1 μm thickness. The front and rear cells are HN and they are referred as H_1 and H_2, while the middle cell is TN with 90° twist angle and it is referred as T. An x-polarized input beam is considered and the losses are neglected. Then, from Eqs. (3)–(5), the transfer function of T_y is

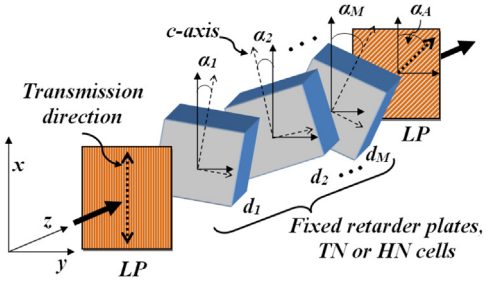

Fig. 4. Achromatic polarization rotator scheme, with M elements, where $d_1 \ldots d_M$ are thickness and $\alpha_1 \ldots \alpha_M$ and α_A are azimuth angles.

given by the element {1,2} of the transfer matrix

$$W = P_x(\alpha_A) \times \ W_{H2}(\alpha_{H2}) \times \ W_T(\alpha_T) \times W_{H1}(\alpha_{H1}) \qquad 8)($$

where P_x is the Jones matrix of the output LP (analyzer) parallel to the x-axis and α_A is its azimuth angle measured from the x-axis [21], as shown in Fig. 4.

The design process objective is to find the best azimuth angle of each LC cell and the analyzer (α_{H1}, α_T, α_{H2} and α_A) to obtain the desired response in the range from 400–700 nm. The optimization is performed by using a Genetic Algorithm (GA) since the random nature of the GA increments the possibility of finding a global minimum; moreover it allows implementing black-box function and the LC experimental characteristics [30], which can be discontinuous and non-differentiable, as part of the objective function. The proposed optimization problem considers only the azimuth angle of each LC cell and the analyzer, $x=[\alpha_{H1}, \alpha_T, \alpha_{H2}, \alpha_A]$ and minimizes the next objective function

$$F_{obj}(x) = \ RMS[T_r - T_y(\lambda, x)] \text{ with } 400\text{ nm} \leq \lambda \leq 700\text{ nm} \qquad (9)$$

where *RMS* represents the root mean square and T_r is the required transmission of T_y that is 1 in this case.

The searching time was 5 s and the optimal values are $\alpha_{H1}=74.76^\circ$, $\alpha_T=-1.56^\circ$, $\alpha_{H2}=12.12^\circ$ and $\alpha_A=86.88^\circ$, obtaining $T_y \geq 99.28\%$ in the range from 400–700 nm, as shown in Fig. 6. The attenuation of the T_x polarization component, represented as $T_x[\text{dB}]=10 \times \log_{10}(1-T_y)$, is shown in the same figure. The result is $T_x[\text{dB}] < -21$ dB in the range from 400–700 nm. $T_x[\text{dB}]$ must be as low as possible. It is important to note that for practical purposes, α_A represents the azimuth angle of the PBS's reflection axis, which is orthogonal to its transmission axis.

This design is as good as previous state-of-the art with more complex designs. The considered LC cells are commercial; this reduces manufacturing tolerances and facilitates the final device construction.

3.2. Broadband 1 × 2 liquid crystal router performance

In this section, the performance of the proposed router is experimentally tested and it is compared against the performance of a router based on a single TN cell of 5CB material, 5.1 μm thickness and 90° twist angle, as the described in Section 2.2, named simple router.

According to the operating principle of the router, in the OFF state, when $V < V_{th}$, S_1 is the inactive output and S_2 is the active output. While in the ON state, when $V \gg V_{th}$, S_1 is the active output and S_2 is the inactive output, as shown in Fig. 5. The optical power of S_1 and S_2 is represented as P_{S1} and P_{S2}, respectively. The router performance is evaluated in terms of insertion loss, IL, and cross-talk, CT. The IL is the ratio of the power transmitted by the active output from the input power, P_{in}, and it is expressed as

$$\text{IL}_{OFF} = -10 \log \left(\frac{P_{S_2}}{P_{in}}\right)_{\text{when } V < Vth} \text{ or}$$

$$\text{IL}_{ON} = -10 \log \left(\frac{P_{S_1}}{P_{in}}\right)_{\text{when } V > > Vth} \qquad (10)$$

On the other hand, CT is the ratio of the power transmitted by the inactive output from the power transmitted by the active output and it is expressed as

$$\text{CT}_{OFF} = 10 \log \left(\frac{P_{S_1}}{P_{S_2}}\right)_{\text{when } V < Vth} \text{ or}$$

$$\text{CT}_{ON} = 10 \log \left(\frac{P_{S_2}}{P_{S_1}}\right)_{\text{when } V > > Vth} \qquad (11)$$

It is important to note that, according to above definitions, IL > 0 dB and CT < 0 dB and they must be as small as possible.

The experimental set-up used to test the router performance is shown in Fig. 7. The LC cells are experimental devices and are mounted on manual rotation mounts. A halogen light source and a spectrometer are used. The fiber optic spectrometer has a 360–890 nm spectral range, and about 4 nm of spectral resolution. Multimode optical fibers and collimators are used at input and output ports. In this characterization, the PBS is replaced by two LPs, which represent the PBS's transmission and reflection axes. This is done in order to avoid moving the spectrometer's fiber, keeping the constant the power reference for the 0% and 100% transmission, which are named dark and white references, respectively. The LPs are from the series WP25M-VIS with operation range from 420–700 nm. For the transmittance calculation, the white reference is taken with parallel LPs and the dark reference is taken with crossed LPs, in order to eliminate the influence of the LPs.

The IL and CT values of the proposed LC-OR are shown in Figs. 8 and 9, respectively. The results are compared with results of

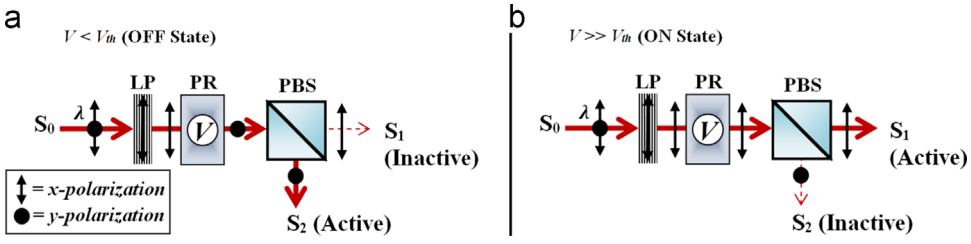

Fig. 5. Scheme of the proposed 1 × 2 LC optical router: a) OFF state and b) ON state. S_0: input port, S_1 and S_2: output ports, V: control voltage and V_{th}: threshold voltage.

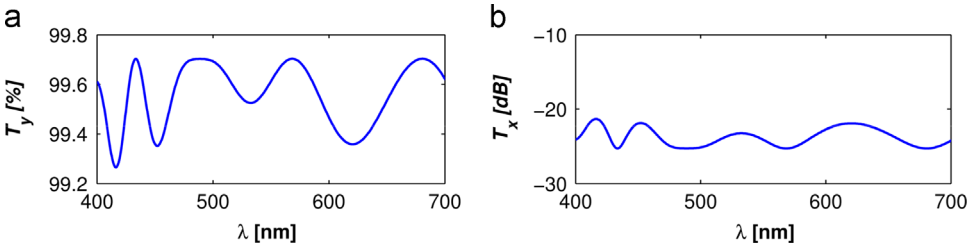

Fig. 6. Theoretical response of the proposed design ($\alpha_{H1}=74.76^\circ$, $\alpha_T=-1.56^\circ$, $\alpha_{H2}=12.12^\circ$ and $\alpha_A=86.88^\circ$): a) transmittance of the T_y polarization component and b) attenuation of the T_x polarization component, $T_x[\text{dB}]=10 \times \log_{10}(1-T_y)$.

the simple LC-OR obtained under the same characterization conditions.

We first analyze the IL of the S_1 output (IL_{ON}) since it does not depend on the PR efficiency, it only depends on the transmittance of the LC cells. As shown in Fig. 8b, the average IL_{ON} of the simple router is 0.84 dB and the average IL_{ON} of the proposed router is 2.74 dB, which is 3.3 times the IL_{ON} of the simple router since it is made by 3 LC cells. On the other hand, the IL of the S_2 output (IL_{OFF}) also includes the effect of the rotation efficiency. Theoreti-cally, if the rotation efficiency is 100%, IL_{OFF}=IL_{ON}. As shown in Fig. 8a, the simple router has average IL_{OFF} of 1.42 dB, which represents a variation of 69% from its average IL_{ON}, while the proposed router has average IL_{OFF} of 2.64 dB, which represents a variation of only 3.6% from its average IL_{ON}.

The CT of the S_2 output (CT_{ON}) does not depend on the PR efficiency, it mainly depends on the capacity of the LC cells to reach $\theta \cong 90^\circ$ when $V \gg V_{th}$ (see Section 2.2). As shown in Fig. 9b, the CT_{ON} of the simple router is lower than −30 dB, while the CT_{ON} of the proposed router is lower than −25 dB. Those values can be regulated applying a lower voltage. On the other hand, the CT of the S_1 output (CT_{OFF}) is mainly defined by the rotation efficiency. As shown in Fig. 9a, the CT_{OFF} of the simple router has a maximum value of −7 dB. This represents a poor performance and a variation of 23 dB from its maximum CT_{ON}. While in the case of the proposed router the CT_{OFF} has maximum value of −18.68 dB.

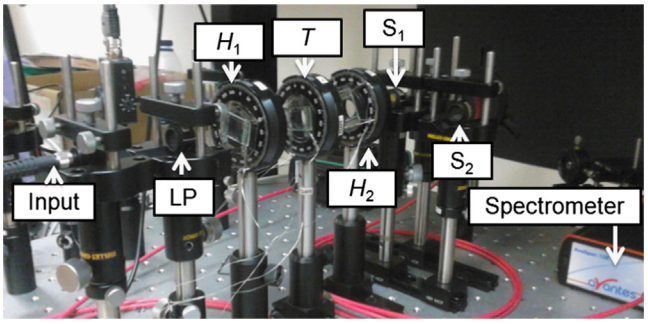

Fig. 7. Experimental set-up. H_1 and H_2 are HN cells and T is a TN cell.

4. Discussion

The proposed PR design allows a significant improvement of the spectral response of LC optical routers, as in those previously reported [10,11,19,20], in a broadband range, and may even improve the response of LC devices reported recently [23]. The experimental results show that the proposed router has quite similar values of IL in both outputs (OFF and ON states) in the range from 400–nm, as well as CT values lower than −18.68 dB. This performance is required for routing channels in SI-POF–WDM networks uniformly [1,2], since in these networks the channels have wide bandwidths (LED sources are often used) and the proposed grid is very wide [3,6–8]. The router improvement has been done without complicating its construction and using commercially available LC cells (fixed thicknesses).

Fig. 10a shows a comparison between the crosstalk in the off state, CT_{OFF}, from the experimental results (see Fig. 9a) and the theoretical design (see Fig. 6b). The shapes of both curves are very similar. However, there are some discrepancies; the experimental curve (solid line) shows a kind of vertical and horizontal offsets, as well as slightly greater amplitude, from the theoretical curve (dashed line). This is because, the theoretical model of Fig. 10a is obtained considering that d_{H1}=d_{H2}=d_T=5.1 μm, ϕ_T=90°, α_{H1}=74.76°, α_T=−1.56°, α_{H2}=12.12° and α_A=86.88° (original design data, see Section 3.1). However, the LC cells used in the set-up are experimental devices and they are mounted on manual rotation stages (see Fig. 7), so it is normal to have some variations from the theoretical values in the experimental set-up. In Fig. 10b an example of how the variations of the theoretical values of the azimuth angles and thicknesses of all the LC cells, as well as the twist angles of the TN cell, can produce a result from the theoretical model more close to the experimental results is shown. The simulation plotted in Fig. 10b (called fitted model) is obtained considering that d_{H1}=5.042 μm, d_{H2}=5.025 μm, d_T=5.080 μm, ϕ_T=86.1°, α_{H1}=74°, α_T=−3°, α_{H2}=11° and α_A=87°. The fitted model shows how the tolerance of some parameters can affect the experimental results. Those values (angles and thicknesses) are obtained using an optimization routine considering reasonable

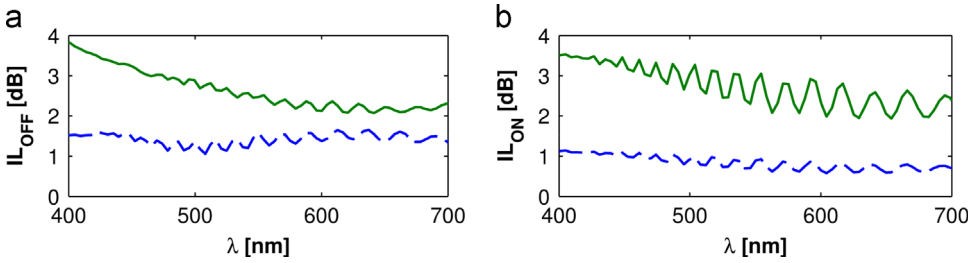

Fig. 8. IL measurements of the proposed router (solid line) and the simple router (dashed line), where: a) IL of the S_2 output ($V < V_{th}$, IL_{OFF}) and b) IL of the S_1 output ($V \gg V_{th}$, IL_{ON}).

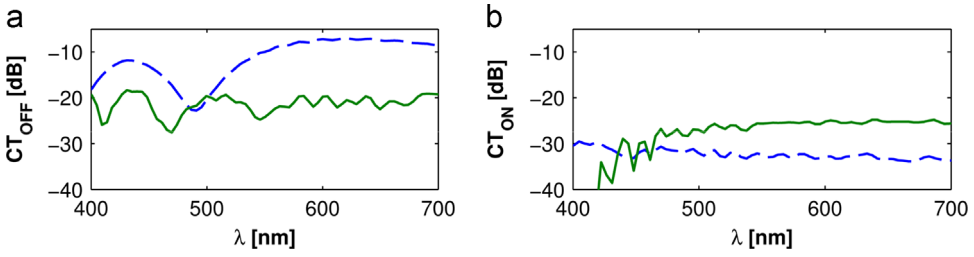

Fig. 9. CT measurements of the proposed router (solid line) and the simple router (dashed line), where: a) CT of the S_1 output ($V < V_{th}$, CT_{OFF}) and b) CT of the S_2 output ($V \gg V_{th}$, CT_{ON}).

tolerances given by the experimental set-up (rotation mounts and LC cells).

It is important to note that the LC cells used do not include any anti-reflection coating. This is one of the factors that cause the ripple of IL (see Fig. 8). The IL and its ripple are mainly caused by the electrodes of Indium Tin Oxide (ITO) of the LC cells. For example, the transmission of a 400 Å thick ITO film is 81% and 95% at 400 nm and 700 nm, respectively [31]. Each LC cell of the proposed router has its own electrodes (6 electrodes in total). Therefore, it would be necessary to use electrodes optimized over the range from 400–700 nm or compact structures in order to reduce the losses [27].

A very important feature of this type of optical router is the ability to control the split ratio of the output power, P_{out}, since $P_{S1}+P_{S2}=P_{out}$. The split ratio is controlled by the applied voltage to the LC cells, which modifies the tilt angle, θ, of the LC molecules between 0° and 90°; see Fig. 2. Fig. 11a shows that the transmittance of the S_2 output of the simple router is very wavelength dependent for intermediate transmission levels (intermediate θ values). However, the proposed router allows intermediate transmission levels, or variable split ratios, with good spectral uniformity in the VIS range, by applying different control voltages to each LC cell, as shown in Fig. 11b. In this Fig. 3 intermediate transmission levels of the S_2 output of the proposed router are shown. For simplicity, the control voltages of each cell are represented as the tilt angles θ_{H1}, θ_T and θ_{H2}, for the cells H_1, T and H_2, respectively. The value of each tilt angle is found with an optimization process similar to the one presented in Section 2.3, maintaining fixed the azimuth angles ($\alpha_{H1}=74.76°$, $\alpha_T=-1.56°$, $\alpha_{H2}=12.12°$ and $\alpha_A=86.88°$) optimizing the vector $\mathbf{x}=[\theta_{H1}, \theta_T, \theta_{H2}]$ in order to obtain the desired transmission levels T_r.

On the other hand, an important drawback of the LC based devices is the strong dependence of the birefringence with the temperature (T). The birefringence of the 5CB material versus the temperature, Δn(T), is presented in [32] at 546 nm, 589 nm and 633 nm. Therefore, the birefringence versus temperature of others wavelengths, Δn(T, λ), can be extrapolated by using the extended Cauchy model [22]. Fig. 12 shows the variation of CT_{OFF} with the temperature of both routers using this approximation of Δn(T, λ). As shown in Fig. 12a, the simple router has optimum CT_{OFF} at 535 nm when the temperature is 20 °C and it shifts to 509 nm and 470 nm when the temperature is 25 °C and 30 °C, respectively. As result, for a fixed wavelength, e.g. at 509 nm, the CT changes between <-20 dB and -10 dB with a variation of only 10 °C. On the other hand, the proposed router has a very low dependence of its CT_{OFF} with the temperature, thanks to its spectral uniformity, as shown in Fig. 12b. The proposed router has a maximum variation of 4 dB in its CT_{OFF} in the range from 400–650 nm for a temperature variation between 20 °C and 30 °C. In the case of the experimental results, the reported values are valid up to 900 nm. Then, if the

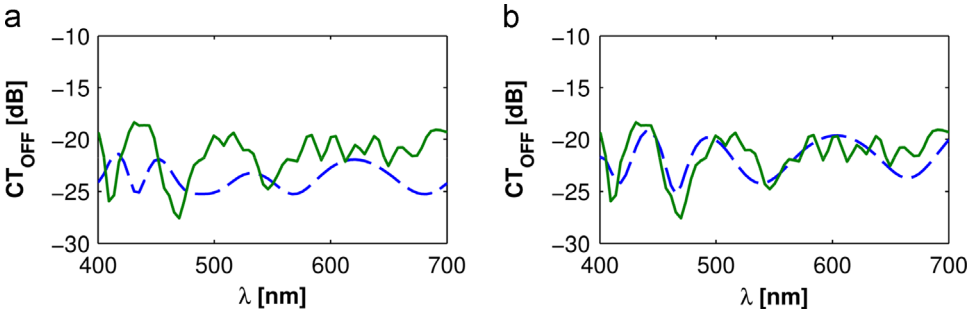

Fig. 10. Theoretical model (dashed line) and experimental results (solid line) comparison a) original design data: $d_{H1}=d_{H2}=d_T=5.1$ μm, $\phi_T=90°$, $\alpha_{H1}=74.76°$, $\alpha_T=-1.56°$, $\alpha_{H2}=12.12°$ and $\alpha_A=86.88°$ and b) fitted model: $d_{H1}=5.042$ μm, $d_{H2}=5.025$ μm, $d_T=5.080$ μm, $\phi_T=86.1°$, $\alpha_{H1}=74°$, $\alpha_T=-3°$, $\alpha_{H2}=11°$ and $\alpha_A=87°$.

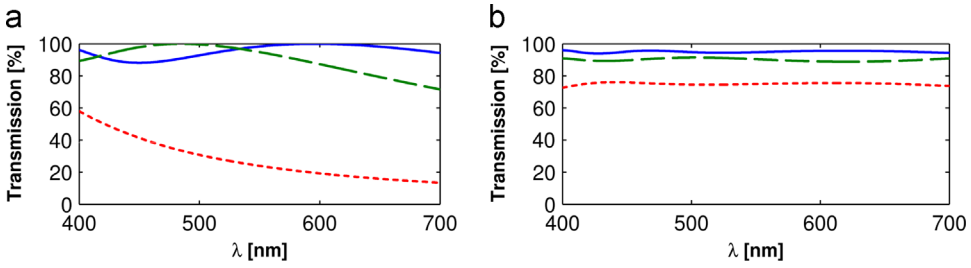

Fig. 11. Intermediate transmission levels of the S_2 output of the: a) simple router with $\theta_T=38.69°$ (solid line), 47.33° (dashed line) and 65.36° (dotted line) and b) proposed broadband router with $[\theta_{H1}, \theta_T, \theta_{H2}]=[41.65°, 38.69°, 38.38°]$, $[47.33°, 47.33°, 51.18°]$ and $[62.36°, 65.36°, 52.06°]$ for $T_r=0.95$, 0.90 and 0.75, respectively. The transmittance effects of the LC cells electrodes are not considered.

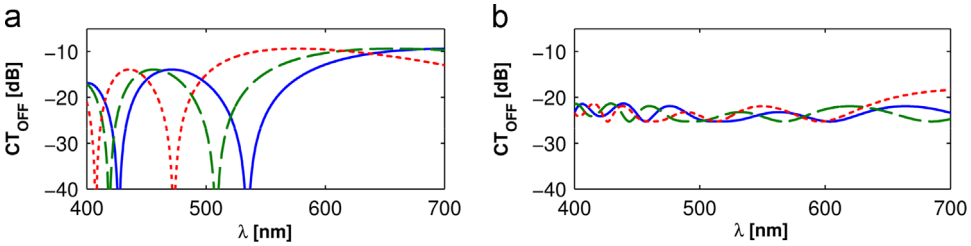

Fig. 12. CT_{OFF} of the a) simple router and b) proposed router at 20 °C (solid line), 25 °C (dashed line) and 30 °C (dotted line).

spectral response is shifted due to a temperature increment, the maximum CT will continue to be less than −18.68 dB.

5. Conclusion

A broadband 1 × 2 optical router based on an achromatic LC PR has been designed and experimentally tested. The PR design process is simple, fast, and produces results comparable with the current state of the art with much more complex designs. The proposed PR design has rotation efficiency $T_y \geq 99.28\%$ in the range from 400–700 nm. The experimental results show that the proposed router has quite similar values of IL and CT in both outputs (OFF and ON states). The router has experimental CT and average IL lower than −18.68 dB and 2.74 dB, respectively, in both outputs, in the range from 400–700 nm. It has been shown that the router performance is quite constant with temperature changes of up to 10 °C. It was also demonstrated that it is able to control the split ratio of the output power with good uniformity in the range from 400–700 nm. We can conclude that this router is a versatile device that allows routing the multiple broadband channels used in WDM networks and sensor systems based in SI-POF.

Acknowledgments

This paper was supported by the Spanish Economy and Education Ministries through grants (Refs. TEC2012-37983-C03-02 and PRX12/00007).

References

[1] U.H.P. Fischer, M. Haupt, M. Jončić, in: P. Predeep (Ed.), Optoelectronics – Devices and Applications, InTech Europe, Rijeka, 2011, p. 445.
[2] L. Bilro, N. Alberto, J.L. Pinto, R. Nogueira, Sensors 12 (2012) 12184.
[3] O. Ziemann, J. Krauser, P.E. Zamzow, W. Daum, POF Handbook: Optical Short Range Transmission Systems, second ed., Springer, New York, 2008.
[4] D.F.C. Lopez, A. Nespola, S. Camatel, S. Abrate, R. Gaudino, J. Lightwave Technol. 27 (2009) 2908.
[5] C.M. Okonkwo, E. Tangdiongga, H. Yang, D. Visani, S. Loquai, R. Kruglov, B. Charbonnier, M. Ouzzif, I. Greiss, O. Ziemann, R. Gaudino, A.M.J. Koonen J. Lightwave Technol. 29 (2011) 186.
[6] O. Ziemman and L.V. Bartkiv, POF–WDM, the Truth, in: Proceedings of the 20th International Conference on Plastic Optical Fibers (Bilbao, Spain, 2011, pp. 525–530.
[7] M. Jončić, M. Haupt, U.H.P. Fischer, Proc. SPIE 9007 (2013) 90070J.
[8] M. Jončić, M. Haupt and U.H.P. Fischer, Investigation on spectral grids for VIS WDM applications over SIPOF, in: Proceedings of the ITG Symposium: Photonic Networks (Leipzing, Germany, 2013, pp. 1–6.
[9] Ray T. Chen, George Ferris Lipscomb. WDM WDM and Photonic Switching Devices for Network Applications: 27–28 January, 2000, San Jose, California *Volumen 3949 de Proceedings of SPIE - The International Society for Optical Engineering*. 184 páginas.
[10] C. Vázquez, I. Pérez, P. Contreras, B. Fracasso, B. Vinouze, in: S.J. Chua, B. Li (Eds.), Optical Switches: Materials and Design, Woodhead Publishing Limited, Gran Bretaña, 2010 (Chapter 8).
[11] P.C. Lallana, C. Vázquez, B. Vinouze, Opt. Commun. 285 (2012) 2802.
[12] M.W. Geis, R.J. Molnar, G.W. Turner, T.M. Lyszczarz, R.M. Osgood, B.R. Kimball, Proc. SPIE 7618 (2010) 1.
[13] D.H. Song, J. Kim, K. Kim, S. Rho, H. Lee, H. Kim, T. Yoon, Opt. Express 20 (2012) 11659.
[14] Y. Ha, H. Kim, H. Park, D. Seo, Opt. Express 20 (2012) 6448.
[15] V. Borshch, S.V. Shiyanovskii, O.D. Lavrentovich, in: J. Rolland, J. Wyant, P. Chavel, X. Zhang, C. Wang, Y. Bai (Eds.), CIOMP–OSA Summer Session on Optical Engineering, Design and Manufacturing, Optical Society of America, 2013 (paper Tu8).
[16] L.P. Amosova, V.N. Vasilev, N.L. Ivanova, E.A. Konshina, J. Opt. Technol. 77 (2010) 79.
[17] V.G. Chigrinov, Crystals 3 (2013) 149.
[18] P. Xu, X. Li, V.G. Chigrinov, Jpn. J. Appl. Phys. 45 (2006) 200.
[19] P.J. Pinzón, I. Pérez, C. Vázquez, J.M.S. Pena, Mol. Cryst. Liq. Cryst. 553 (2012) 36.
[20] C. Vázquez, J.M.S. Pena, S.E. Vargas, L.A. Aranda, I. Pérez, IEEE Sens. J. 3 (2003) 513.
[21] Pochi Yeh, Claire Gu, Optics of Liquid Crystal Displays, second ed., John Wiley & Sons, New York, 2010.
[22] J. Li, C. Wen, S. Gauza, R. Lu, S. Wu, J. Disp. Technol. 1 (2005) 51.
[23] M. Decker, C. Kremers, A. Minovich, I. Staude, A.E. Miroshnichenko, D. Chigrin, D.N. Neshev, C. Jagadish, Y.S. Kivshar, Opt. Express 21 (2013) 8879.
[24] Q. Wang, T.X. Wu, X. Zhu, S. Wu, Liq. Cryst. 31 (2004) 535.
[25] Qian Wang, Gerald Farrell, Thomas Freir, Jun She, J. Opt. A 7 (2005) (2005) 47.
[26] A.B. Golovin, O.P. Pishnyak, S.V. Shiyanovskii, O.D. Lavrentovich, Proc. SPIE 6135 (2006) 61350E.
[27] R.K. Komanduri, K.F. Lawler, M.J. Escuti, Opt. Express 21 (2013) 404.
[28] Z. Zhuang, Y.J. Kim, J.S. Patel, Appl. Phys. Lett. 76 (2000) 3995.
[29] P.J. Pinzón, C. Vázquez, I. Pérez, J.M. Sánchez, IEEE Photon. J. 5 (2013) 7100113.
[30] B. Ma, B. Yao, T. Ye, M. Lei, J. Appl. Phys. 107 (2010) 073107.
[31] I.-C. Khoo, S.-T. Wu, Optics and Nonlinear Optics of Liquid Crystals, World Scientific, New Jersey, 1993.
[32] J. Li, S. Gauza, S. Wu, J. Appl. Phys. 96 (2004) 19.